Challenging Glass Conference Proceedings – Volume 10 – June 2026 – Louter, Bos & Belis (Eds.)
International Conference on the Architectural and Structural Application of Glass
Challenging Glass Conference 10 – 15-17 June 2026 – TU Delft – The Netherlands

# Compliance of Pillars in a Vacuum Insulated Glass

**Christian Alter [a], Cenk Kocer [b], David McKenzie [b]**

a Technische Hochschule Mittelhessen, Giessen, Germany, christian.alter@me.thm.de
b University of Sydney, School of Physics, Sydney, NSW, Australia, cenk.kocer@sydney.edu.au

## Abstract

This paper presents an analytical framework for characterising the lateral compliance of a cylindrical column constrained between deformable elastic substrates, with direct application to the contact mechanics of pillars used in vacuum insulating glass (VIG) units; these pillars support the glass panes as a set of discrete array points over the glass surface to maintain separation under atmospheric pressure. Under combined normal and lateral loading, four physically distinct deformation mechanisms were found to contribute to total pillar (column) compliance: column bending, column shear, rigid-body rotation driven by asymmetric substrate indentation, and surface shear of the substrate at the contact interface. Using Timoshenko beam theory for a column, Fabrikant's flat-punch tilting solution for rotational compliance, and contact mechanics solutions for surface shear, the total lateral compliance is expressed as a closed-form superposition. The analytical predictions are validated against three-dimensional finite element models across column heights of 0.1 to 0.5 mm and radii of 0.15 to 0.5 mm with excellent agreement over all cases. This framework will enable rapid parametric optimisation of the pillar geometry in VIG design for any external load configurations.

## Keywords

Vacuum Insulated Glass, Pillar compliance, Beam theory, Contact mechanics, Finite Element Analysis

## Article Information

- Digital Object Identifier (DOI): 10.47982/cgc.10.767
- Published by Challenging Glass, on behalf of the author(s), at Stichting OpenAccess.
- Published as part of the peer-reviewed Challenging Glass Conference Proceedings, Volume 10, June 2026, 10.47982/cgc.10
- Editors: Christian Louter, Freek Bos & Jan Belis

## 1. Introduction

Vacuum insulating glass (VIG) is a high-performance glazing technology in which two glass panes are separated by a narrow evacuated gap, which is typically 0.1 to 0.3 mm wide; an illustration of the VIG structure is provided in figure 1 (Collins 1998). The VIG is associated with thermal transmittance values substantially lower than those achievable with conventional double or triple glazing, at a much thinner profile and lower overall weight. The structural integrity of a VIG unit depends critically on a regular array of small cylindrical support pillars that maintain the gap width between the glass panes, against atmospheric pressure acting over the two panes. In all VIG designs the pillars are the sole load-carrying elements between the panes, and thus, must be designed such that the pillars do not yield/break or initiate fracture of the glass under in-service loads, while remaining small enough in cross-section to limit heat flow between the panes.

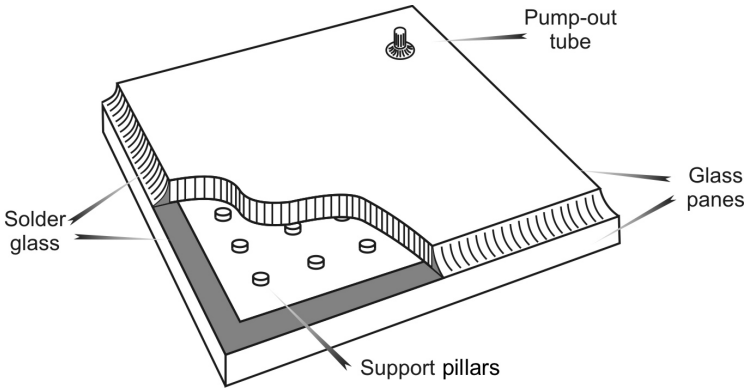


Fig. 1: An illustration of the Vacuum Insulated Glass (VIG) (Collins 1998).

The mechanical loading environment of a VIG pillar is more complex than simple axial compression. Bending of the VIG, and thus the glass panes, under external loading such as wind, thermal difference, or impact, produces relative tangential displacement of the inner glass surfaces at each pillar location, imposing lateral shear forces on the pillar end faces. These lateral forces are superimposed on the permanent axial compression from atmospheric pressure where the axial compression depends on the pillar separation distance and the cross-section size of the pillar. The combined loading drives localised contact stresses at the pillar-glass interface that govern the structural integrity of the glass, and therefore, the VIG unit.

Despite the practical importance of pillar compliance in VIG systems, no closed-form analytical solution describing the full lateral compliance of the equivalent cylindrical column sandwiched between elastic substrates appears in the literature. Finite element analysis (FEA) can resolve individual configurations, but is a time consuming and complex process to undertake for broad parametric sweeps required during design optimisation. Classical beam theory, in either Euler-Bernoulli or Timoshenko (1921) form, addresses column deformation in isolation but neglects the deformability of the supporting substrates, which, as demonstrated here, can contribute 30 to 60 percent of the total lateral compliance for VIG-relevant geometries.

Contact mechanics solutions are available for several relevant sub-problems independently: normal indentation of an elastic half-space by a flat-ended punch (Sneddon 1965), tilting of a circular punch under an applied moment (Fabrikant 1988, Karapetian et al. 2000), and tangential loading of a circular contact under full-stick conditions (Popov 2010). The contribution of the present work is to assemble these results, together with Timoshenko beam theory (Timoshenko 1921), into a single coherent

superposition framework that captures all four operative deformation modes and is validated over the full range of geometries relevant to VIG pillar design. The resulting closed-form compliance expressions enable instantaneous evaluation of any combination of height, radius, and material, supporting systematic optimisation of the trade-off between structural compliance and thermal bridging.

## 2. Problem Formulation

As an equivalent pillar geometry system, consider a cylindrical column of height $l$and radius $r$, with Young's modulus $E_c$, shear modulus $G_c$, and Poisson's ratio $\nu_c$. The column is compressed between two planar elastic substrates, which is the glass panes with moduli $E_s$, $G_s$, and Poisson's ratio $\nu_s$, by an applied axial force $P$, while simultaneously subjected to a lateral force $F$ applied at one substrate face, in the direction transverse to the column axis. The axial coordinate $x$ runs from 0 to $l$along the column axis, and $w(x)$denotes the transverse displacement field. Both end contacts are modelled under full-stick conditions and separation from the substrate is not permitted.

A key physical complication in this setup is that the substrate end conditions are not rigid: each contact face can undergo normal indentation, tangential sliding, and/or rotation. These deformations feed back into the column boundary conditions, coupling the structural and contact-mechanics sub-problems. Relating the lateral deflection, four independent deformation mechanisms are identified, each amenable to an analytical solution, and their compliance contributions can be superposed to give the total system compliance.

## 3. Analytical Framework: Superposition of Deformation Modes

The total lateral displacement of one substrate face relative to the other, denoted $\bar{w}$, is decomposed into four additive contributions:

$$\bar{w} = \bar{w}_b + \bar{w}_s + \bar{w}_r + \bar{w}_f \qquad (1)$$

where $\bar{w}_b$ is the end displacement due to column bending, $\bar{w}_s$ due to column shear, $\bar{w}_r$ due to rigid-body rotation of the column caused by asymmetric substrate indentation, and $\bar{w}_f$ due to tangential surface shear deformation of the substrate at the contact interfaces, where each mode is illustrated in Figure 2.

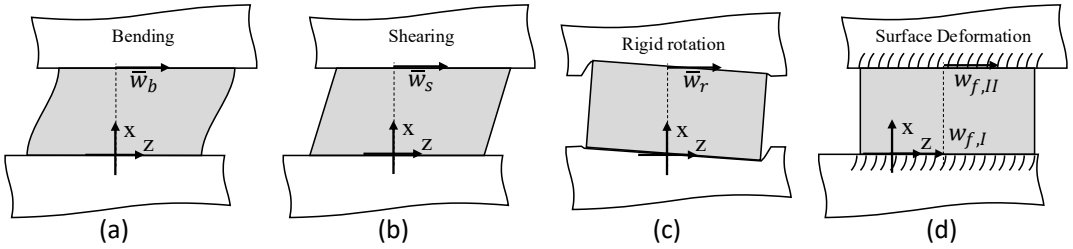


Fig. 2: The four independent deformation modes contributing to total lateral compliance. (a) Column bending under an internal moment *M(x)*. (b) Column shear under constant internal shear force *F*. (c) Rigid-body rotation of the column arising from asymmetric substrate indentation by the contact moment. (d) Surface shear deformation of the substrate at each pillar-substrate interface.

Compliance $C$ is defined as the ratio of end displacement to lateral force, $C = \bar{w}/F$, so that total compliance is:

$$C_{tot} = C_b + C_s + C_r + C_f \tag{2}$$

## 3.1. Column Bending and Shear (Timoshenko Beam Theory)

Adopting Timoshenko beam theory, the cross-section rotation $dw/dx$ consists of shear deformation $\gamma$ and bending deformation $\varphi$. The mean shear strain in the cross-section is then given as,

$$\gamma(x) = \frac{dw}{dx} + \varphi(x). \tag{3}$$

For zero distributed transverse load along the column, the equilibrium equations reduce to,

$$E_c I_c \frac{d^4 w_b}{dx^4} = 0, \tag{4}$$

$$\kappa G_c A_c \frac{d^2 w_s}{dx^2} = 0 \tag{5}$$

where $I_c = \pi r^4/4$ is the second moment of area, $A_c = \pi r^2$ is the cross-sectional area, and $\kappa$ is the Timoshenko shear correction factor. Following Cowper (1966)

$$\kappa = \frac{6(1+\nu_c)}{(7+6\nu_c)} \tag{6}$$

for a solid circular cross-section is used.

Equations (4) and (5) are solved subject to boundary conditions at $x = 0$: $w = 0$ and $\varphi = -\theta$ (the substrate tilt angle), and at $x = l$: $d^3 w_b/dx^3 = -F/(E_c I_c)$ and $\varphi = -\theta$ (the substrate tilt angle at the far end). The tilt angle $\theta$ is determined by the contact mechanics described in Section 3.2.

The bending and shear compliance contributions are then,

$$C_b^r = \frac{l^3}{(12\, E_c\, I_c)}, \tag{7}$$

$$C_s = \frac{l}{(\kappa\, G_c\, A_c)} \tag{8}$$

where the superscript $r$ in $C_b^r$ denotes the contribution that would arise with rigid substrate end conditions (i.e. no end rotation permitted). The rotational contribution $C_r$ adds to this, as described next.

## 3.2. Rigid-Body Rotation from Substrate Indentation

The bending moment $M(x)$ at each contact face creates an asymmetric contact pressure distribution, causing one side of the contact circle to penetrate more deeply into the substrate than the other. This differential indentation produces a rigid tilt of the column end face. For a circular flat-ended punch of radius r in contact with an isotropic elastic half-space (Young's modulus $E_s$, Poisson's ratio $\nu_s$), the tilt angle $\theta$ produced by a tilting moment $M$ is given by the solution of Fabrikant (1988) and Karapetian et al. (2000)

$$\theta = \frac{3(1-\nu_s^2)\,M}{(4\,r^3 E_s)}. \tag{9}$$

The tilting moments at the two contact faces are obtained from beam theory: $M_{t,0} = -E_c I_c\, d^2 w_b/dx^2|_{x=0} = M_{t,l} = E_c I_c\, d^2 w_b/dx^2|_{x=l}$ These moments provide the tilt angle $\theta$ used as boundary conditions in Section 3.1. The resulting rotational compliance is then given as,

$$C_r = \frac{3(1-\nu_s^2)\,l^2}{(8\,E_s\,r^3)}. \tag{10}$$

This term scales as $l^2$ (quadratic in column height) and $r^{-3}$ (strong inverse-cubic radius dependence), making it particularly significant at moderate aspect ratios.

## 3.3. Substrate Surface Shear

The lateral force $F$ must be transmitted tangentially across each column-substrate contact. Treating the column as rigid relative to the substrate ($G_c \to \infty$) and assuming full-stick conditions over the circular contact area of radius *r*, the tangential displacement of an elastic half-space under lateral force $F$ is,

$$w_f = \frac{F}{2\,G^*\,r} \tag{11}$$

where $G^*$ is the equivalent contact shear modulus, combining the properties of both bodies in contact,

$$\frac{1}{G^*} = \frac{(2-\nu_c)}{(4G_c)} + \frac{(2-\nu_s)}{(4G_s)}. \tag{12}$$

In the rigid-column limit ($G_c \to \infty$), the second term vanishes and $G^*$ is determined solely by the substrate shear modulus $G_s$ and its Poisson's ratio $\nu_s$leading to a surface shear compliance of

$$C_f = \frac{1}{(G^*\,r)}. \tag{13}$$

Crucially, $C_f$ is independent of column height $l$; it represents a fixed compliance floor that dominates the response of short columns; typically the pillars in VIG units are considered short since they are wider than their height, for example, the typical cylindrical pillar is 0.5 mm in diameter and 0.2 mm in height.

## 3.4. Total Compliance

Combining Equations (7), (8), (10), and (13), the total lateral compliance of the column-substrate system will be given as,

$$C_{tot} = \frac{l^3}{(12\,E_c I_c)} + \frac{3(1-\nu_s^2)\,l^2}{(8\,E_s\,r^3)} + \frac{l}{(\kappa\,G_c\,A_c)} + \frac{1}{(G^*\,r)}. \tag{14}$$

This is the central result of this work. Each term is directly traceable to a physical mechanism, enabling mode-by-mode sensitivity analysis and targeted design optimisation. The compliance contributions in order in equation (14) are left-to-right, bending ($C_b^r$), rigid rotation ($C_r$), column shear ($C_s$), and surface shear ($C_f$).

## 4. Finite Element Modeling Validation

Three-dimensional finite element models were constructed using the explicit solver of ANSYS LS-DYNA to validate the analytical framework. A coincident-node approach was adopted at the column-substrate interfaces to enforce full-stick contact without the artificial compliance associated with penalty-based contact formulations. All materials were treated as linear elastic and the values used in the models are in Table 1. The optimum element size was determined through a convergence study, with mesh refinement concentrated at the contact perimeter where stress gradients are steepest.

Table 1: Linear elastic material properties for glass substrates and steel columns used in the FEM simulations.

| Material | Young's Modulus [MPa] | Poisson's ratio [-] |
|---|---|---|
| Glass (Substrate) | 70,000 | 0.23 |
| Steel (Column) | 210,000 | 0.33 |

The four-mode superposition was validated against FEM simulations of the full coupled system: a steel column sandwiched between two identical glass substrates, with both column deformation and substrate deformation included. In the simulations the column radii 0.15, 0.20, 0.25, and 0.50 mm, at heights from 0.10 mm to 0.50 mm were modelled. Figure 3 compares the total compliance $C_{tot}$ predicted by Equation (14) with the FEM simulation results. Agreement between the analytical and FEM results is good across the full range, including at height-to-diameter ratios as low as 0.2:1, well below the regime where Euler-Bernoulli theory would be adequate. The Timoshenko shear correction, Equation (6), is essential at these low aspect ratios, where column shear contributes strongly to the total column compliance. Mode-by-mode FEM comparisons indicate that Timoshenko beam theory provides a good approximation of transverse-shear effects even at low $l/r$ ratios; as aspect ratios become low, the bending contribution to the total deformation in the presented approach decreases, where the overall compliance remains in good agreement with the 3D FEM results.

The analytical model captures the full compliance behaviour across four column radii and four height values, spanning more than one order of magnitude in compliance. The agreement is good validation that the four deformation modes constitute the relevant set of mechanisms under the current loading configuration, and that linear superposition is correct.

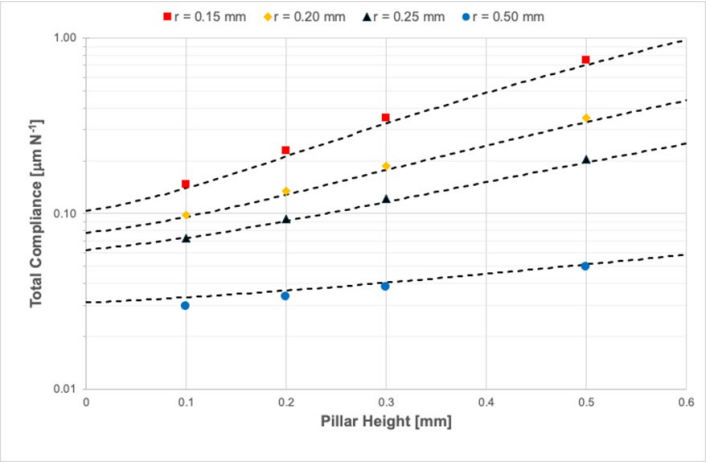


Fig. 3: Total lateral compliance$C_{tot}$ (Equation 14) as a function of column height l for four column radii. Lines: analytical superposition. Points: FEM simulation results. Log scale on compliance axis. Steel column, symmetric glass-substrate case.

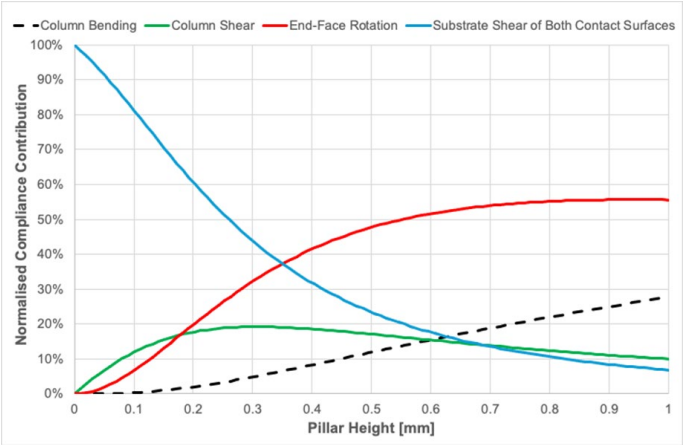


Fig. 4: Normalised compliance contributions of the four deformation modes as a function of pillar height $l$, for $r = 0.2$ mm and $E_c/E_s = 3$. Column bending $C_b$ (black dashed line); column shear $C_s$ (green line); rigid-body rotation $C_r$ (red line); substrate surface shear of both end faces $C_f$ (blue line).

Parametric sweeps over axial force (10–253 N) and lateral force (1–126 N) show negligible variation in lateral compliance within the linear range; the presented plots are for 10 N of axial force and 1 N of lateral force.

The success of the linear superposition is itself a non-trivial result. The four modes are not geometrically independent - rotation of a column end modifies the bending field, and surface shear of the substrate displaces the effective boundary condition for the column. The fact that the superposition nonetheless works accurately reflects the mathematical structure of the problem: for linear elastic materials under small deformations, the principle of superposition holds rigorously, and cross-coupling terms between modes vanish to first order. This justifies the decomposition approach and gives confidence that the framework will remain accurate for geometries and material combinations beyond those explicitly tested here.

From a practical standpoint, this validation result means that a designer can evaluate the total lateral compliance of a VIG pillar configuration in a single algebraic calculation, rather than commissioning a purpose-built FEM study for each candidate geometry. For a design sweep over, say, five candidate radii and ten candidate heights, this reduces the computational effort from potentially days of FEM model building and post-processing to a few seconds of spreadsheet evaluation.

## 5. Discussion

Figure 4 is a plot of the relative contribution of each compliance mode to the total $C_{tot}$ as a function of column height, for a column/pillar of radius $r$ =0.2 mm where $E_c/E_s = 3$ (steel pillar and glass substrate). The dominant mechanism transitions progressively from surface shear at low heights through rotation and column shear to bending at large heights.

The scaling relationships governing these transitions are summarised in Table 3. For VIG pillars with heights in the range 0.1 to 0.3 mm, substrate surface shear $C_f$ contributes more than 50 percent of the total compliance. This finding is structurally significant: the glass substrate itself, not the steel pillar, is the primary source of lateral flexibility in a short VIG pillar. Any model that treats the glass as a rigid boundary condition will predict a compliance roughly half of the true value, leading to non-conservative predictions of contact stress and glass fracture risk.

Table 2: Scaling of each compliance contribution with column height l and radius r. The hierarchy of exponents on l explains why surface shear dominates for short pillars and bending dominates for tall ones. The hierarchy of exponents on r shows that increasing r is most effective for reducing bending, and least effective for reducing surface shear.

| Mode | Height scaling | Radius scaling | Dominant regime |
|---|---|---|---|
| Bending $C_b$ | $C_b \propto l^3$ | $C_b \propto r^{-4}$ | Tall, slender pillars |
| Rotation $C_r$ | $C_r \propto l^2$ | $C_r \propto r^{-3}$ | Moderate aspect ratio |
| Shear $C_s$ | $C_s \propto l$ | $C_s \propto r^{-2}$ | Low to moderate heights |
| Surface shear $C_f$ | - | $C_f \propto r^{-1}$ | Short pillars (e.g. typical VIG gap height) |

The rotation mode, $C_r$, deserves particular attention because it is the most physically subtle contribution. It is not a deformation of the column but a rigid tilt of the entire column arising from the asymmetric deformation of the glass substrate under the moment produced at the contact surface. Its quadratic height dependence means that its contribution grows faster than the shear component (which is linear) but slower than bending (which is cubic), making it most prominent at intermediate aspect ratios. For a pillar of radius 0.2 mm and at height 0.5 mm (an aspect ratio of 2.5:1), rotation contributes approximately 20 to 30 percent to the total compliance. Omitting this mode leads to a systematic underestimate across the geometrically common moderate-height range.

The compliance framework does more than quantify pillar-glass system stiffness, it fully specifies the contact boundary value problem, enabling a closed-form analytical chain from macroscopic external loading of the VIG unit to the glass contact stress. Because the surface-shear compliance term takes the form $C_f = 1/G^* r$, the contact radius is fixed by pillar geometry alone, independent of load magnitude in the case of the most used cylindrical geometry. At the pillar-glass contact shear force $F$ and tilting moment $M_t = (Fl)/2$, are both functions of the applied lateral force. Knowledge of these parameters is to use the classic flat-punch contact solutions - Sneddon's (1965) pressure distribution for the axial preload $P$, Mindlin's (1949) tangential traction for the shear $F$, and Fabrikant's (1988) antisymmetric tilt term for $M_t$ — each sharing the same $\frac{1}{\sqrt{1-\left[\frac{x}{r}\right]^2}}$ functional form.

The practical consequence is that the peak tensile surface stress at the contact perimeter, which governs crack growth over the service life of the VIG unit, becomes an explicit function of $F, P, r, l, E_s$ and $\nu_s$ alone. For example, in the simplest case substituting into a Mode I stress intensity factor $K_I = Y\sigma_{peak}\sqrt{(\pi c)}$ (where this is assuming a surface flaw geometry represented by the factor $Y$ and uniform stress distribution over the flaw length) and a power-law crack growth model, we have a design pathway in closed form. A geometry change - adjusting pillar radius or height - propagates analytically through the compliance expressions, updates the contact resultants, and revises the failure prediction, with no new finite element model required at any stage. The compliance framework thus serves as the single analytical bridge connecting the macroscopic structural response of the glazing unit to the microscopic contact mechanics that control its long-term integrity (Fang et al. 2014).

Although the validation presented here is for the steel-glass material combination relevant to VIG, the framework is general. Any system in which a cylindrical element is loaded laterally while compressed between two deformable layers falls within the scope of Equation (14). Examples include: solder bumps and copper spacers in flip-chip electronic packages, where coefficient of thermal expansion mismatch drives lateral fatigue loading between chip and substrate; ceramic spacers in solid oxide fuel

cell stacks, where operational thermal cycling imposes lateral displacements between electrode layers; contact pads in MEMS sensors and actuators, where substrate compliance is comparable to element stiffness; and bearing spacers in precision optical instruments, where lateral stiffness determines alignment stability under thermal or mechanical perturbation.

The explicit inclusion of substrate deformability also has implications for how experimental compliance measurements should be interpreted. If compliance is measured between two substrate faces and the substrate contribution is not subtracted, inferred column material properties will be in error. The framework provides the analytical correction: given a measured total compliance $C_{tot}$ and known substrate properties, the column-only compliance $C_b + C_s$ is extracted by subtracting $C_r + C_f$ analytically. This is directly useful in material characterisation of small columns tested in sandwich configurations, which is standard practice in both MEMS research and hard coating indentation studies.

## 6. Conclusion

A closed-form analytical solution for the total lateral compliance of a cylindrical column sandwiched between two elastic substrates has been presented in this work and validated. The key conclusions are:

1. The lateral compliance is completely described by the linear superposition of four deformation modes: column bending, column shear, rigid-body rotation from asymmetric substrate indentation, and substrate surface shear. No additional modes are required.
2. Established analytical solutions (Timoshenko beam theory (Timoshenko 1921), Fabrikant's tilting contact (Fabrikant 1988), Popov's tangential contact (Popov 2010)) provide closed-form expressions for each mode. Their superposition, Equation (14), yields the total compliance.
3. Three-dimensional FEM simulations confirm the accuracy of the model for column heights $l = 0.1$ to 0.5 mm and contact radii of $r = 0.15$ to 0.5 mm, covering the full practical VIG pillar range.
4. Substrate surface shear compliance, $C_f = 1/(G^* r)$, dominates for short pillars ($l <$ 0.2 mm), contributing over 50 percent of total displacement. This component is entirely absent from rigid-substrate beam models.


## Acknowledgements

This research was conducted using resources of the National Computing Infrastructure (NCI) HPC 'Gadi', an NCRIS-enabled capability supported by the Australian Government. Access to these resources was provided by the Sydney Informatics Hub, a Core Research Facility of The University of Sydney, as supported by the Deputy Vice-Chancellor (Research).


## References


Collins, R. E., Simko, T. M:. Current status of the science and technology of vacuum glazing. Solar Energy, 62(3), 189–213 (1998)

Cowper, G. R.: The shear coefficient in Timoshenko's beam theory. Journal of Applied Mechanics, 33(2), 335–340 (1966)

Fabrikant, V. I.: Elastic field around a flat punch. Journal of Applied Mechanics, 55(3), 604–610 (1988)

Fang, Y., et al.: Vacuum insulated glazing - a review of the thermal performance, challenges and future directions. Applied Energy, 197, 422–435 (2014)

Karapetian, E., Kachanov, M., Sevostianov, I.: The elastic field due to a hemispherical contact on a half-space. Journal of the Mechanics and Physics of Solids, 48(1), 169–186 (2000)

Mindlin, R. D.: Compliance of elastic bodies in contact. Journal of Applied Mechanics, 16, 259–268 (1949)

Popov, V. L.: Contact Mechanics and Friction: Physical Principles and Applications. Springer (2010)

Sneddon, I. N.: The relation between load and penetration in the axisymmetric Boussinesq problem for a punch of arbitrary profile. International Journal of Engineering Science, 3(1), 47–57 (1965)

Timoshenko, S. P.: On the correction for shear of the differential equation for transverse vibrations of prismatic bars. Philosophical Magazine, 41(245), 744–746 (1921)

Challenging Glass Conference Proceedings – Volume 10 – June 2026 – Louter, Bos & Belis (Eds.)
International Conference on the Architectural and Structural Application of Glass
Challenging Glass Conference 10 – 15-17 June 2026 – TU Delft – The Netherlands

## Platinum Sponsor

SAINT-GOBAIN

## Gold Sponsors

EASTMAN

kuraray

NorthGlass®

sedak

seele

## Silver Sponsors

DOW®

octatube

PERMASTEELISA GROUP

SEEN

## Organisation

TU Delft

Technische Universität München

GHENT UNIVERSITY